

# Design and Realization of Electromagnetic Energy Harvesters

Che-Ming Lee and Wei-Jiun Su\*

Department of Mechanical Engineering, National Taiwan University, Taipei, Taiwan

## Abstract

In this article, we discuss a novel electromagnetic energy harvester that combines a BLDC and a ball screw inerter. The inerter is a complete two-terminal mechanical device, which can be equivalent to the mass in the mechanical system, so that the mechanical network system can be perfectly matched to the electronic network system. Inerter has been successfully applied to the suspension of automobiles, trains and buildings. Therefore, we design this electromagnetic energy harvester to verify its mechanical model and energy harvesting power. Because it contains many uncertainties, such as the friction force. We fit these unknown parameters in the experimental part and then explores the impact of the damping and the inertance on the energy harvester. In the end, the energy harvester is used in the building for vibration reduction. The Tuned Mass Damper (TMD) is a common method of vibration control. Because the stroke of the TMD is greater than the displacement of the structure, and the energy of vibration will be dissipated to heat. In recent years, some scholars have begun to add the inerter to the TMD device as a Tuned Mass Damper Inerter (TMDI). The electromagnetic energy harvester designed in this thesis will be used as an inerter in TMDI, and its damping effect is verified by numerical simulation. The simulation results show that under the earthquake and the wind load, this energy harvesting-enabled tuned mass-damper-inerter (EH-TMDI) device, not only can effectively reduce the vibration of the structure, but also can collect considerable electrical energy.

**Keywords:** Electromagnetic Energy Harvester, Inerter, Tuned Mass Damper, Tuned Mass Damper Inerter

## 1 Introduction

Generally, the damping design in the suspension system dissipates the vibration energy from the ground disturbance into heat, but the heat dissipated in the environment cannot be reused. The waste of its thermal energy will cause the energy use efficiency to be low, which is unfavorable to the sustainable development of the environment and energy. Due to the disturbance of the road surface isolated by the car suspension system or the earthquake and strong wind isolated by the building suspension system, it is a source of energy that can continuously provide vibration energy, so it is very suitable for the application of vibration energy harvester to form energy-regenerative suspension systems [1]. The energy-regenerative suspension systems combines an energy harvester with a shock absorber. The vibration energy is shunted from the damping into its electronic network system, enabling it to recover energy and reduce vibration in the suspension system. Among them, electromagnetic energy harvesting is suitable for environments with large amplitude. The electromagnetic motor can play the role of driver and harvester at the same time, and can be reduced to a mathematical model of voltage source series inductance and motor internal resistance [2], so electromagnetic energy harvesting shock absorbers often used in suspension systems, especially in electromagnetic suspension systems (EMS), enables them to recover energy or have a self-powered system. In this paper, the electromagnetic energy harvester used in large-scale systems is divided into linear electromagnetic energy harvester and rotary electromagnetic energy harvester according to its transmission mode.

Early Karnopp designed an electrodynamic variable shock absorbers with a permanent magnet linear motor inside and applied to the vehicle suspension [3]. The permanent magnet linear actuator was also used by Martins et al. in electromagnetic active suspension and compared with hydraulic active suspension [4]. Suda et al. mainly studied self-powered active vibration control systems, starting with hybrid suspension systems.

---

\*Corresponding author. Email: weijiunsu@ntu.edu.tw

The passive suspension in this hybrid suspension uses an energy regenerative damping system that converts vibrational energy into usable energy and supplies it to active control to balance the energy consumption of active control in improving suspension performance [5]. Self-powered active vibration control systems using two linear motors are also used for suspension in truck cabins, and suspension performance is superior to passive or semi-active suspension [6]. The research team also used a single electric actuator to achieve active control and energy regeneration [7]. Gupta et al. designed an energy-renewable electromagnetic shock absorber [8]. Soon after, many scholars invested in different types of linear electromagnetic energy harvesters. Gysen et al. explored the efficiency and energy consumption of a regenerative direct-drive electromagnetic active suspension [9]. Chen et al. improved the traditional magnetorheological damper, abandoned the power supply and velocity sensor in the traditional magnetorheological damper, and designed self-sensing magnetorheological damper with power generation which can sense the relative velocity [10]. Zuo et al. designed a linear electromagnetic energy harvester for vehicle suspensions and experimentally measured its energy harvesting power [11]. In 2014, his research team, Tang et al., designed a tubular linear electromagnetic vibration energy harvester [12]. Linear electromagnetic energy harvesters can not only be used in vehicle suspensions, but also in the damping of a tuned mass damper (TMD). Recently, Yuan et al. designed a non-traditional vibration absorber that can simultaneously serve as vibration suspension and energy harvesting [13]. Different from the traditional TMD in which the absorber damper is attached to the primary mass, this non-traditional TMD has electromagnetic damping connected between the absorber mass and the ground. The study shows that When the vibration absorber reaches the optimal state, the frequency response function of the main mass can be nearly flat in a wider frequency band, and the purpose of energy harvesting is achieved.

In order to improve the damping coefficient of the linear electromagnetic energy harvester, some scholars began to design a rotary electromagnetic energy harvester. Such electromagnetic energy harvesters can be divided into rack-pinion type, ball screw type and other special mechanisms according to their structural components. Li et al. combined the rack-pinion mechanism to design an electromagnetic energy harvesting shock absorber and actually tested it on the road [14]. Although the damping coefficient of this energy harvesting damper is used in vehicle suspensions, the backlash problem also results in lower mechanical efficiency relative to other devices. In order to improve the mechanical efficiency, the research team added a one-way clutch into the mechanism design, making it a mechanical motion rectifier (MMR) [15]. In addition to the commonly used in vehicle suspensions, electromagnetic energy harvesters using rack-pinion mechanisms can also be used in building vibration damping systems such as TMD [16], as well as railway applications such as train suspension systems [17], vibration energy harvesting of the railroad tracks [18, 19] and so on. Liu et al. also used the rack-pinion type of rotary electromagnetic energy harvester to design an energy harvesting paver [20], which can harvest the vibration energy generated by pedestrians when walking. The ball screw is another mechanism commonly used to convert linear motion into rotation. Compared to the rack and pinion mechanism, the backlash has less influence. Kawamoto et al. combined a permanent magnet motor with a ball screw mechanism to create an electromagnetic damper that can be used in a vehicle suspension to increase the damping effect and recover the energy consumed [21,22]. Zhang et al. experimentally verified the feasibility of an energy regenerative automotive electrical suspension system which matched the ball screw and nut with a permanent magnet DC brushless motor. The device can be switched into a mode of driving, braking and energy regeneration [23]. The energy harvester designed by Cassidy et al. combines a ball screw with a permanent magnet synchronous motor [24] and applies it to large structures such as buildings and bridges. The research team also used statistical linearization to optimize this energy harvester [25]. Wai et al. applied a ball screw energy regenerative damper to an electric vehicle, which enabled the electric vehicle to have an energy harvesting system [26]. Recently, Liu et al. designed an energy harvesting shock absorber with mechatronic inerter properties and added a one-way clutch as a MMR, and applied it to the automotive suspension system [27]. Unlike the rack-pinion and ball screw type, Maravandi et al. use a motion converter called a two-legged mechanism. Such a mechanism has the advantages of simple design, low friction and high efficiency [28].

In terms of improving the damping effect, in addition to changing the different transmission modes, adding an inerter is also an option. An inerter is an ideal mechanical two-terminal element, which is a substitute for the mass element in mechanical/electrical analogy. Since the invention of an inerter, this new mechanical component has been used repeatedly in various types of suspensions, and can successfully improve the performance of the suspension. Inerters can be mechanically realised in various ways. Until now, four realisations of inerters

have been presented [29–36]. If the inerter is added to the TMD, it is a new type of passive vibration control device, which can also be called a tuned mass-damper-inerter (TMDI). Marian and Giaralis first proposed this concept in 2014. TMDI takes full advantage of the mass amplification effect of the inerter, and the best designed TMDI is superior to the traditional TMD. Therefore, the passive components can replace part of the TMD primary mass to achieve a lightweight passive vibration control solution [37]. Soon after, Salvi and Giaralis proposed the concept of combining TMDI with energy harvester, which can be used for both vibration suppression and energy harvesting, that is, energy harvesting-enabled tuned mass-damper-inerter (EH-TMDI). There are two main configurations, the first one is the electromagnetic motor connected to the energy harvester in series and the grounding inerter, while the TMDI mass part has a linear spring damper attached to the main structure and connected in parallel, the second is the TMDI mass is connected to the grounded inerter and then paralleled to the electromagnetic motor, linear spring and damper. This EH-TMDI adjusts the weight between vibration control and energy harvesting, and optimizes the dual targets [38]. Recently, Marian and Giaralis further proposed TMDI for harmonic vibrations suppression and optimized its additional mass and energy harvesting [39]. Hung et al. proposed an electromagnetic multiple tuned mass damper (EM-MTMD). MTMD is arranged in parallel with multiple TMD units, which can suppress wider frequency bandwidth and provide more robust control effects. In order to improve the viscous damper in the MTMD system, EM-MTMD replaces the traditional viscous damper with an electromagnetic motor, and can also be used as an electromagnetic energy harvester. The rack-pinion mechanism can be expanded to increase its stroke of the damper, and the inertance is taken into account when optimizing its control theory [40]. Luo et al. recently proposed an electromagnetic resonant shunt tuned mass-damper-inerter (ERS-TMDI) for the wind vibration control of buildings, in order to minimize structural damage and simultaneously harvest energy under random wind excitation [41].

In this paper, an electromagnetic energy harvester combining ball screw inerter and mechatronic inerter is designed, which can change the inertance by replacing the flywheel. In addition to the use of impedance changes to achieve vibration reduction, the flywheel can also be changed to tune the inertance. Since the electromagnetic energy harvester can be simplified as electromagnetic damping in parallel with the inerter, it can be added to the TMD to simultaneously add the inerter and the energy harvester. It is also an EH-TMDI. The electromagnetic energy harvester designed in this article utilizes the displacement of TMD mass much larger than the displacement of the primary structure to achieve a win-win effect of simultaneous vibration reduction and energy recovery. In addition to verifying the mechanical model and energy harvesting power of the proposed electromagnetic energy harvester with the input displacement of the dynamic testing machine, this article also analyzes its energy harvesting efficiency and damping effect used in EH-TMDI by numerical simulation. This paper is arranged as follows. In Section 2, a mechanical model is proposed by considering uncertain factors. In Section 3, the experimental setup is shown and the uncertain factors can be tuned by comparing the experimental and theoretical data. Then verify the complete mechanical model of the harvester and finally explore its efficiency. In Section 4, an EH-TMDI system model will be built and evaluated for the effect of the proposed electromagnetic energy harvester in EH-TMDI. Finally, some conclusions are drawn in Section 5.

## 2 Design and Dynamic System

### 2.1 Working Principle

Since the proposed electromagnetic energy harvester includes the ball screw inerter and mechatronic inerter, and the inertance of the ball screw inerter must be adjusted in the experiment, the energy harvester must be specially designed to facilitate the experiment. As shown in Figure 1(a), the energy harvester is mainly divided into two parts, which are a moving end that is connected to the ball screw nut and a fixed end that is connected to the ball screw and the rotor of the gearbox. When the prototype is placed in a dynamic testing machine for experiments, the chuck of the moving end can be clamped by the hydraulic clamp of the dynamic testing machine. Since the hydraulic clamp can be controlled by the dynamic testing machine, the vertical displacement is controlled. Therefore, the nut can be driven by the outer casing connected to the nut to make a linear motion. If we control the displacement of the nut to linear reciprocating motion, it can be regarded as inputting vibration

energy to the prototype, and the vibration energy can drive the nut to move linearly. Due to the characteristics of the ball screw mechanism, if the nut moves in a straight line, the screw will rotate accordingly, and then the fixed end of the flywheel and the permanent magnet motor will rotate, and the induced current is also generated, indicating that the vibration energy is converted into electric energy. At the same time, the purpose of vibration reduction and energy collection is achieved. Finally, according to the above design method, the coupling is combined with a brushless motor (42BLDC030-PB05), a ball screw (MISUMI-C-BSSC1210) and a flywheel, and then the outer casing is manufactured. The prototype of the paper, Figure 2(a) and the nut part of Figure 2(b) are the moving end of the prototype, the screw, flywheel in Figure 2(b) and the brushless motor in Figure 2(c) is connected to the fixed end, and Figure 1(b) is the built prototype. The parameters of the prototype are listed in Table 1.

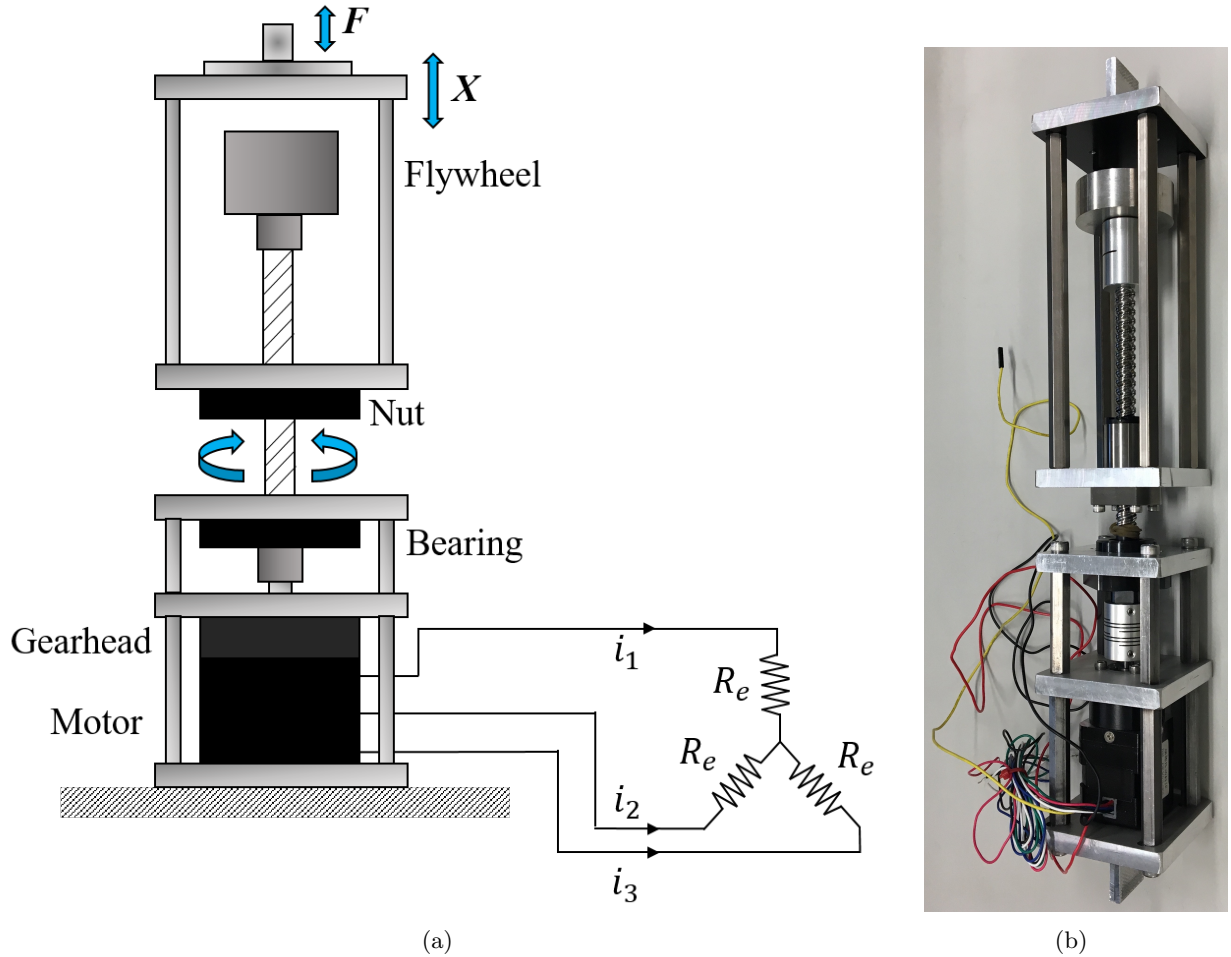
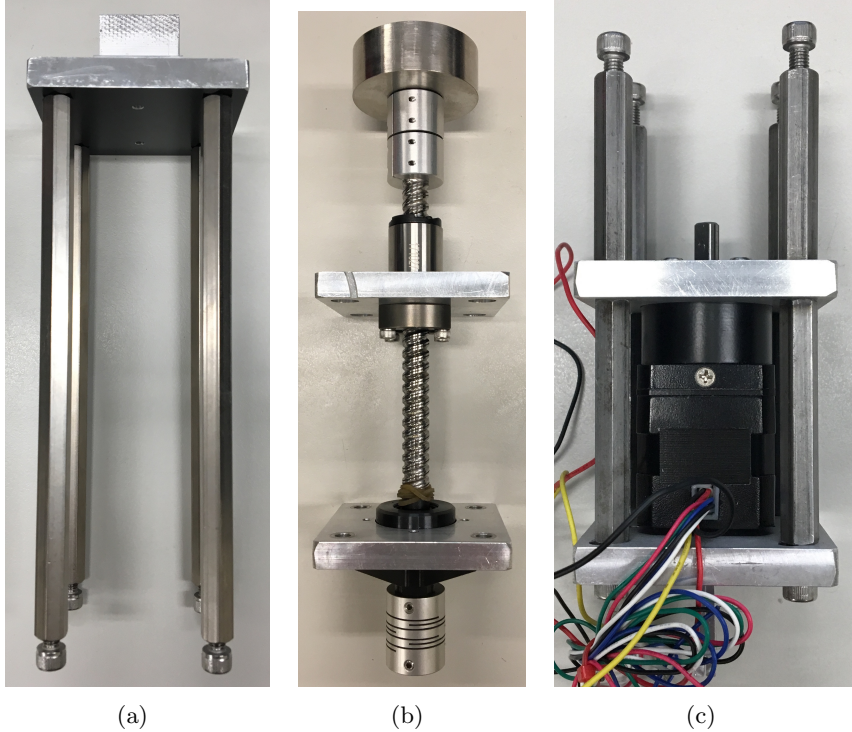


Figure 1: The design of an energy harvester with inerter using a ball-screw mechanism (a) Design drawing (b) Built prototype



(a)

(b)

(c)

Figure 2: The exploded view of the proposed energy harvester (a) Moving part (b) Ball-screw inerter part (c) BLDC part

Table 1: The parameters of the prototype

Parameters	Values	Description
$m_{move}$	1051 [g]	Mass of the moving case
$J_{cp}$	50 [ $\text{g}\cdot\text{cm}^2$ ]	Coupling inertia
$J_{bs}$	60 [ $\text{g}\cdot\text{cm}^2$ ]	Ball-screw inertia
$p$	10 [mm]	Ball-screw pitch
$d_m$	12.3 [mm]	Ball-screw diameter
$f$	0.1	Ball-screw friction factor
$r_g$	5	Generator gearbox ratio
$k_e$	0.028 [V·s/rad]	Generator voltage constant
$k_t$	0.028 [V·s/rad]	Generator torque constant
$J_m$	80 [ $\text{g}\cdot\text{cm}^2$ ]	Generator inertia
$p_{motor}$	8	Generator pole
$n$	3	Generator phase number
$R_i$	2.7 [ $\Omega$ ]	Internal resistance per phase
$L$	3.4 [mH]	Internal inductance per phase

## 2.2 Modeling and Dynamics

Figure 3(a) show the working principle of the linear motion part of the prototype. Since the ball screw used in the experiment is not an ideal screw, the uncertainty factor must be taken into account. In this paper, the friction force  $F_{fric}$  and the friction coefficient  $f$  are added as uncertain factors according to the reference [33, 42, 43]. The relationship between the input force  $F$  and the screw torque  $T$  considering the uncertain factors can be expressed as

$$F = \frac{2}{d_m} \left( \frac{\pi d_m + fp}{p - \pi f d_m} \right) T + m_{move} \frac{d^2 x}{dt^2} + F_{fric} \quad (1)$$

where  $x$  is the displacement input to the prototype,  $p$  is ball-screw pitch,  $d_m$  is ball-screw diameter, and  $m_{move}$  is Mass of the moving case. Since the screw torque will drive the flywheel and the motor to rotate, the operation mode can be expressed by Figure 3(b), which can be written as

$$T = (J_{bs} + J_{fw} + J_{cp}) \frac{d\omega_g}{dt} + T_m \quad (2)$$

where  $J_{bs}$ ,  $J_{fw}$ ,  $J_{cp}$  are the inertia of the screw, flywheel and coupling respectively. Because the three are connected, the three angular velocities are equal to the angular velocity of the gearbox rotor  $\omega_g$ , and  $T_m$  is the torque input to the rotor of the motor.

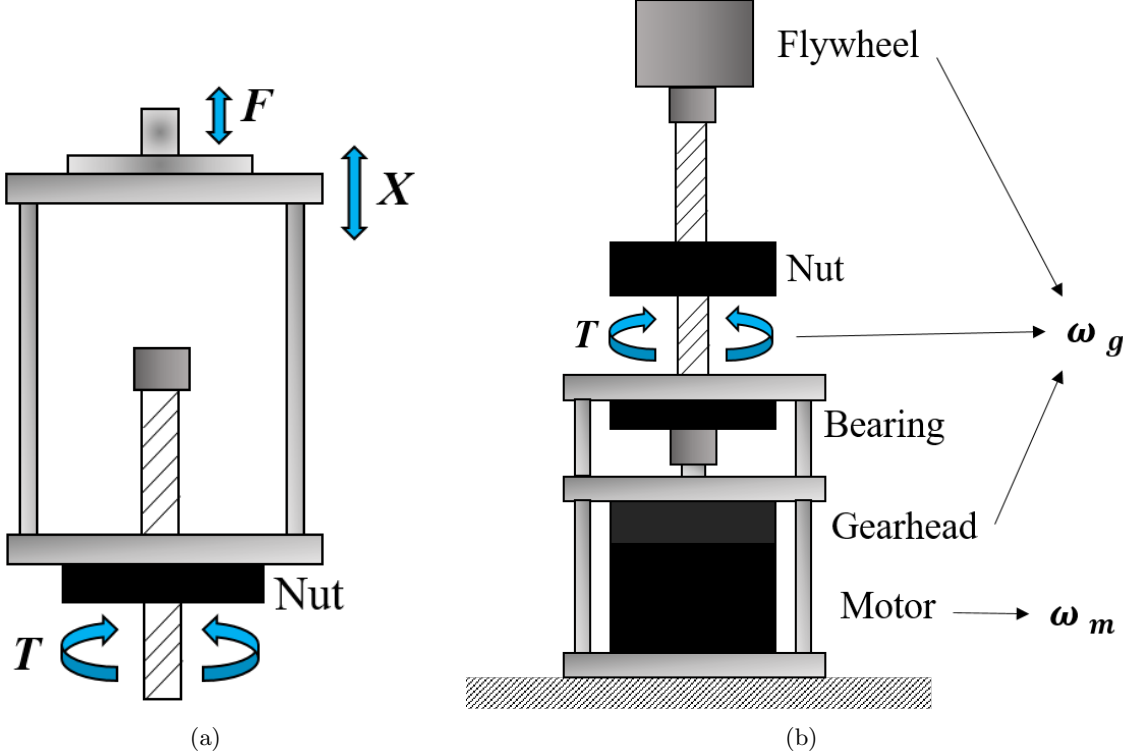


Figure 3: The working principle diagram (a) Linear motion part (b) Rotating motion part

However, this torque  $T_m$  cannot be directly expressed by the inertia of the motor rotor  $J_m$  and its angular velocity  $\omega_m$ . Since the motor generates the induced torque  $T_{emf}$  and the friction torque  $T_{fric}$ , the relationship between  $T_m$  and  $\omega_m$  can be expressed as

$$T_m - T_{emf} - T_{fric} = J_m \frac{d\omega_m}{dt} \quad (3)$$

where  $T_{emf} = k_t \cdot i$  and  $T_{fric} = B_m \cdot \omega_m$ . Since the permanent magnet motor specification used in this prototype does not provide the motor damping coefficient  $B_m$ , it is also an uncertain factor to be considered for this prototype.

In order to obtain the dynamic system model of this prototype, we must derive the relationship between the induced current  $i$  and the angular velocity of the motor rotor  $\omega_m$ . Figure 4 shows the permanent magnet brushless DC motor (BLDC) selected for this prototype. The working principle of power generation used by generators, where  $V_1$ ,  $V_2$  and  $V_3$  are the induced electromotive forces generated by the generator phases,  $i_1$ ,  $i_2$  and  $i_3$  are the induced currents of each phase of the generator,  $L$  and  $R_i$  are the internal inductance and internal resistance per phase,  $R_e$  is the external load of each phase. The induced electromotive force for each phase is [28]

$$V_1 = V_{emf} \cos \left( \omega_e t - \frac{2\pi}{3} \right) \quad (4a)$$

$$V_2 = V_{emf} \cos (\omega_e t) \quad (4b)$$

$$V_3 = V_{emf} \cos \left( \omega_e t + \frac{2\pi}{3} \right) \quad (4c)$$

where  $V_{emf}$  and  $\omega_e$  are the voltage amplitude and angular frequency of the induced electromotive force for each phase, and the relationship between  $V_{emf}$  and  $\omega_m$  is  $V_{emf} = k_e \cdot \omega_m$ . The voltage angular frequency of the induced electromotive force for each phase can be written as

$$\omega_e = \omega_g \cdot r_g \cdot p_{motor} \cdot n \quad (5)$$

where  $p_{motor}$  is the motor pole and  $n$  is the motor phase number. Ignoring the influence of the internal inductance  $L$ , the induced current per phase can be expressed by

$$i_1 = \frac{k_e \cdot \omega_g \cdot r_g \cos \left( \omega_e t - \frac{2\pi}{3} \right)}{R_i + R_e} \quad (6a)$$

$$i_2 = \frac{k_e \cdot \omega_g \cdot r_g \cos (\omega_e t)}{R_i + R_e} \quad (6b)$$

$$i_3 = \frac{k_e \cdot \omega_g \cdot r_g \cos \left( \omega_e t + \frac{2\pi}{3} \right)}{R_i + R_e} \quad (6c)$$

And the sum of the instantaneous electric powers of the three phases  $P_{total}$  can be expressed as [28]

$$P_{total} = \frac{V_1^2 + V_2^2 + V_3^2}{R_i + R_e} \quad (7)$$

Then, substituting Equations 4 into Equation 7 and  $R_i + R_e$  as the sum of resistances  $R$ , the equation can be written as

$$P_{total} = \frac{1.5V_{emf}^2}{R} = \frac{3k_e^2\omega_m^2}{2R} \quad (8)$$

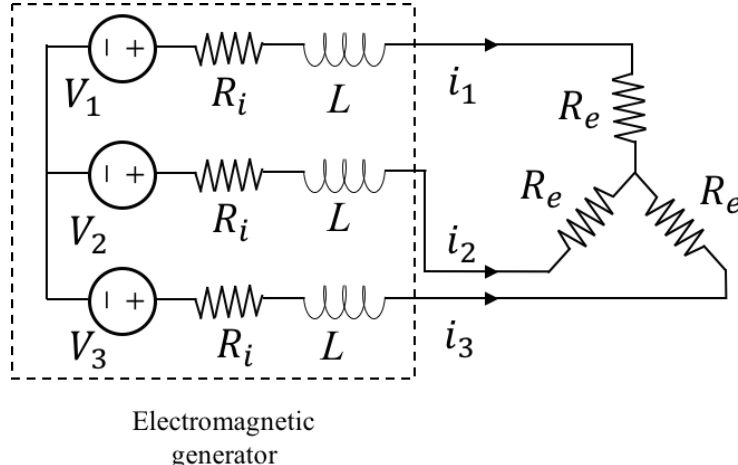


Figure 4: The dynamic model of a three-phase permanent magnet BLDC

Since the external load in Figure 4 uses the Y-connection method, its line current will be equal to the phase current, that is,  $i_1 = i_2 = i_3 = i$ , and this system is equivalent to the mechanical network system, then three-phase transmission. The resistance torque caused by the rotational damping of the motor, that is, the induced torque  $T_{emf}$ , can be expressed by  $B_r \cdot \omega_m$  where  $B_r$  is rotational damping coefficient. Considering the conservation of energy in mechanical and electronic network systems [28], the sum of the instantaneous electric powers of the three phases is

$$P_{total} = T_{emf} \cdot \omega_m = k_t \cdot i \cdot \omega_m \quad (9)$$

Since the  $k_e$  and  $k_t$  of the permanent magnet motor are usually equal, the induced torque of the three-phase generator can be expressed as [27]

$$T_{emf} = \frac{3k_e k_t}{2R} \omega_m \quad (10)$$

After determining the relationship between the induced current  $i$  and the angular velocity of the motor rotor  $\omega_m$ , the relationship between  $\omega_g$  and  $\omega_m$  in Figure 3(b) and the reduction ratio  $r_g$  can be expressed as  $\omega_m = r_g \cdot \omega_g$ . By substituting Equation 3 and 10 into Equation 2, the dynamic system model of the energy harvester in the rotating motion part is

$$T = (J_{bs} + J_{fw} + J_{cp} + J_m + r_g) \frac{d\omega_g}{dt} + \left( \frac{3k_e k_t}{2R} + B_m \right) r_g \omega_g \quad (11)$$

Finally, the part of the linear motion is considered into the dynamics, that is,  $\omega = (2\pi/p)v$  and Equation 11 are substituted into Equation 1, and the theoretical model of the prototype can be written as

$$F = \frac{2}{d_m} \left( \frac{\pi d_m + fp}{p - \pi f d_m} \right) \frac{2\pi}{p} \left[ (J_{bs} + J_{fw} + J_{cp} + J_m + r_g) \frac{d^2x}{dt^2} + \left( \frac{3k_e k_t}{2R} + B_m \right) r_g \frac{dx}{dt} \right] + m_{move} \frac{d^2x}{dt^2} + F_{fric} \quad (12)$$

For convenience, this paper defines the theoretical model as  $F = m_e \frac{d^2x}{dt^2} + c_e \frac{dx}{dt} + F_{fric}$  where the equivalent mass  $m_e$  of this prototype is  $m_e = b + m_{move}$  and the equivalent inertance  $b$  and damping  $c_e$  are

$$b = \frac{2}{d_m} \left( \frac{\pi d_m + fp}{p - \pi f d_m} \right) \frac{2\pi}{p} (J_{bs} + J_{fw} + J_{cp} + J_m + r_g) \quad (13)$$

$$c_e = \frac{2}{d_m} \left( \frac{\pi d_m + fp}{p - \pi f d_m} \right) \frac{2\pi}{p} \left( \frac{3k_e k_t}{2R} + B_m \right) r_g \quad (14)$$

### 3 Lab Tests and Analysis

#### 3.1 Experimental Setup

The experimental setup is shown in Figure 5. The relative displacement in the experiment is the vibration energy of the input energy harvester, which is generated by a dynamic testing machine and can generate sinusoidal displacements of different frequencies and amplitudes. The oscilloscope measures the voltage value of the external resistor connected to the electromagnetic motor, and calculates the harvesting power by the resistance value and the voltage value. The part that verifies the vibration damping effect is measured by the load cell and the displacement meter included in the dynamic testing machine. This machine can output the experimental data of the force and displacement during the experiment, which can be compared with the simulation result. Then we can find the friction force of the ball screw and the motor damping coefficient of the electromagnetic motor, and observe the effect of changing the external resistance and the inertance, and calculate the equivalent damping value of the electromagnetic energy harvester.

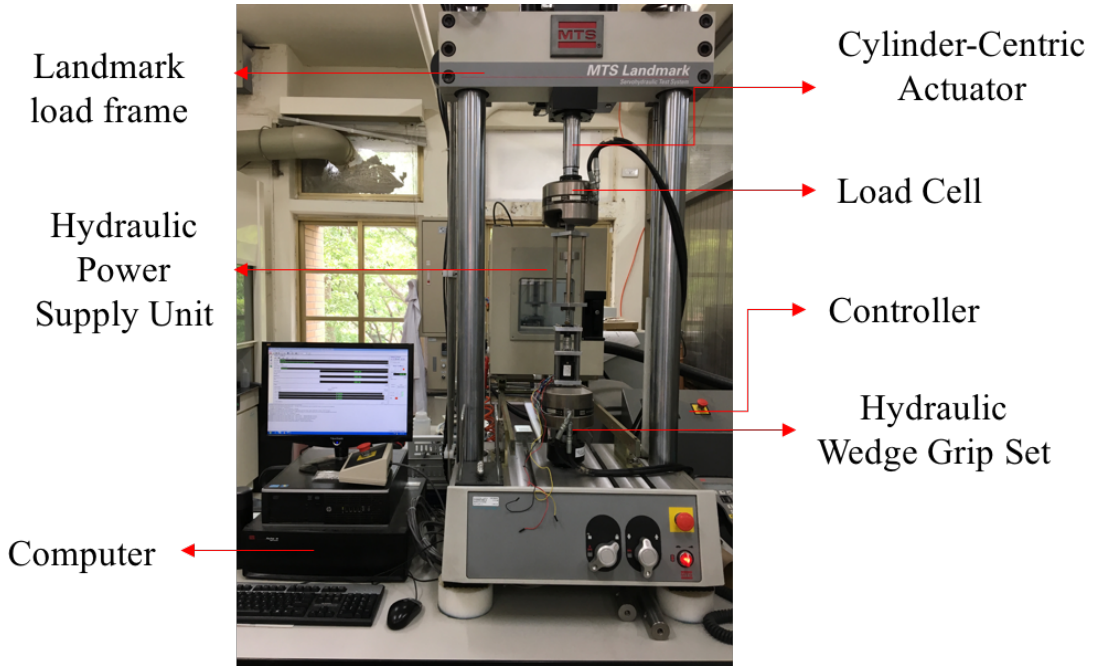


Figure 5: Experimental setup

### 3.2 Force-Displacement Loops and Damping Characteristics

#### 3.2.1 Friction force and motor damping coefficient

After combining the ball screw with the three-phase brushless DC motor, we must first find out the parameters that affect the friction force of the ball screw. Since the ball screw does not have the parameters related to the friction force specified in the specification, it must be analyzed experimentally. We use Stribeck friction as the model of friction force, and it can be written as [43]

$$F_{fric} = \left[ F_c + (F_s - F_c) \exp^{-|\frac{dx}{dt}|/v_s} \right] \cdot \text{sign} \left( \frac{dx}{dt} \right) + F_v \frac{dx}{dt} \quad (15)$$

where  $F_c$  is Coulomb friction,  $F_s$  is the static friction,  $v_s$  is Stribeck velocity, and  $F_v$  is the damping coefficient for this friction model. In addition to the frictional force, the brushless motor specification does not provide the motor damping coefficient  $B_m$ , so the motor damping coefficient needs to be obtained experimentally. The vibration inputs from dynamic testing machine are sinusoidal vibration inputs. It can be written as  $x = A \sin \omega t$  where  $A$  is the amplitude and  $\omega$  is the angular frequency of the sinusoidal vibration input.

Figure 6(a) shows the force-displacement loops of the ball screw under harmonic vibration inputs of  $\omega=0.1\text{Hz}$  for different excitation amplitudes. Figure 6(b) shows the force-displacement loops of the proposed energy harvester under harmonic vibration inputs of  $\omega=2\text{Hz}$  for different excitation amplitudes with open loop circuit. The results are used for fitting the friction force and the motor damping coefficient which are listed in Table 2.

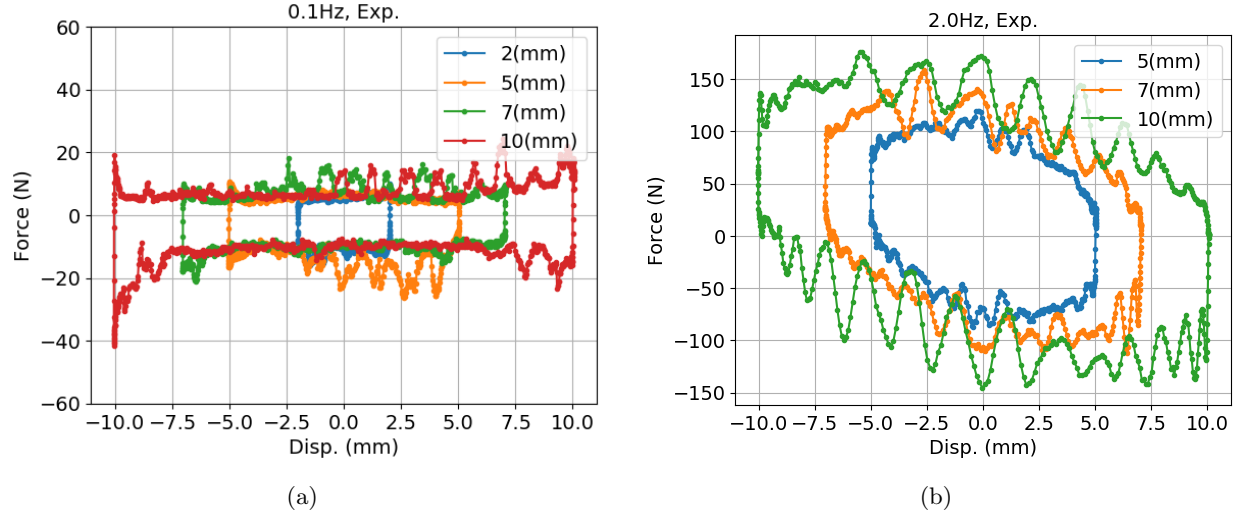


Figure 6: Force-displacement loops under harmonic vibration inputs (a) Only ball-screw (b) Open loop

Table 2: The uncertain factors of the prototype

Parameters	Values	Description
$F_c$	14.4 [N]	Coulomb friction
$F_s$	18 [N]	Static friction
$F_v$	0.0025 [N·s/m]	Damping coefficient for Stribeck friction model
$v_s$	2.3 [mm/s]	Stribeck velocity
$B_m$	0.0005 [N·m·s/rad]	Motor damping coefficient

### 3.2.2 External resistance and inertance

After determining the uncertain factors such as friction force and motor damping coefficient, all parameters of the theoretical model of the prototype of the energy harvester have been determined. This section will discuss the connection of external resistors to form a closed circuit, and change the external resistance value to observe the relationship of force and displacement. It can be seen from the results of experiment in Figure 7 that the smaller the external resistance value, the greater the required input force to achieve the same displacement. And it can be seen from Equation 14 that the smaller the external resistance value, the larger the equivalent damping value of the harvester. The results can also be seen from the elliptical area of the force versus displacement plot of the experimental results from Figure 7. The detailed results of experiment and simulation can be seen in Figure 8.

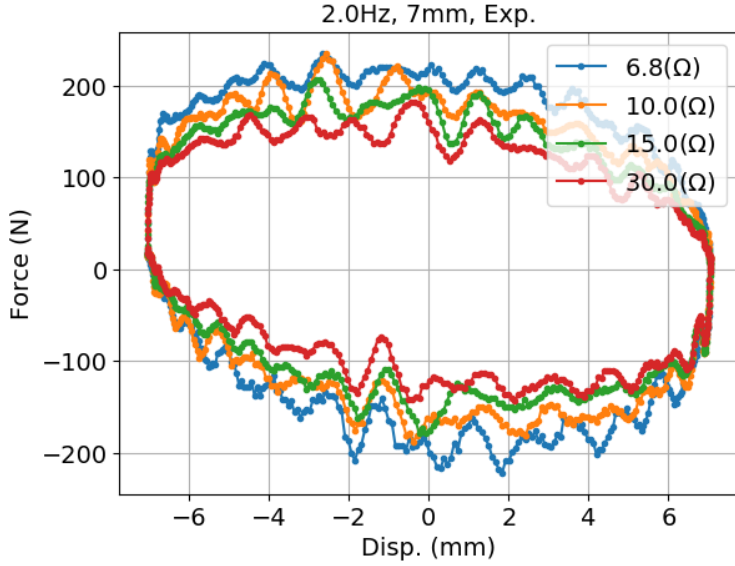


Figure 7: The results of external resistance values under harmonic vibration inputs of  $A=7\text{mm}$ ,  $\omega=2\text{Hz}$

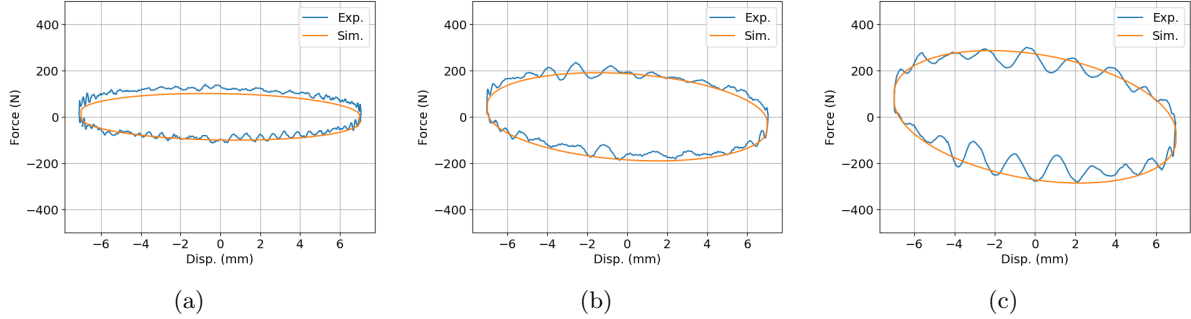


Figure 8: Force-displacement loops under harmonic vibration inputs of  $A=7\text{mm}$  for (a)  $\omega=1\text{Hz}$  (b)  $\omega=2\text{Hz}$  (c)  $\omega=3\text{Hz}$  with external electrical load  $R_e=10\Omega$ .

After completing the above experiment, in the end, this section will install the flywheel on the proposed energy harvester, change its inertance, and compare the changes after changing the inertance. The parameters of the two flywheels in the experiment are listed in Table 3. Although the mass of the two flywheels is less than 400g, the equivalent mass of about 100kg can be produced under the ball screw selected in this paper. As long as the flywheel shape is adjusted so that its moment of inertia is large enough, such as the flywheel 2, even if its mass is slightly lighter than the flywheel 1, its inertance can be greater than that of the flywheel 1. Figure 8, 9 and 10 are the results of the experiment with external load  $R_e=10\Omega$ . Comparing these three sets of pictures, it can be seen that under the input sinusoidal displacement, the change of the inertance mainly affects the equivalent stiffness of the energy harvester, that is, the larger the inertance, the larger the slope of the ellipse under the force of the displacement loop. In other words, the greater the equivalent mass and the inertance can be used to adjust the equivalent mass of the energy harvester. Therefore, when the proposed energy harvester of this paper needs to adjust its equivalent mass to optimize its effect of vibration reduction, the advantage of adding inerter is revealed. Since the inerter has a small increase in the mass of the flywheel, the equivalent mass can be greatly improved, so it is easy to achieve a lot when the equivalent mass is adjusted to optimize the vibration damping effect.

Table 3: The parameters of the flywheels

Parameters	Flywheel 1	Flywheel 2	Units	Description
$m$	398.4	383.2	[g]	Mass
$J_{fw}$	932	1425	[g· cm <sup>2</sup> ]	Moment of inertia
$b$	95.18	127.72	[kg]	Inertance

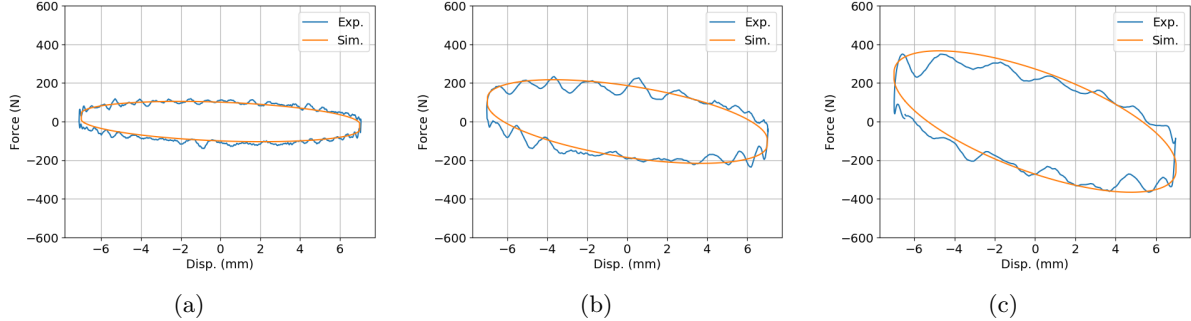


Figure 9: Force-displacement loops under harmonic vibration inputs of  $A=7\text{mm}$  for (a)  $\omega=1\text{Hz}$  (b)  $\omega=2\text{Hz}$  (c)  $\omega=3\text{Hz}$  with external electrical load  $R_e=10\Omega$  and the flywheel 1.

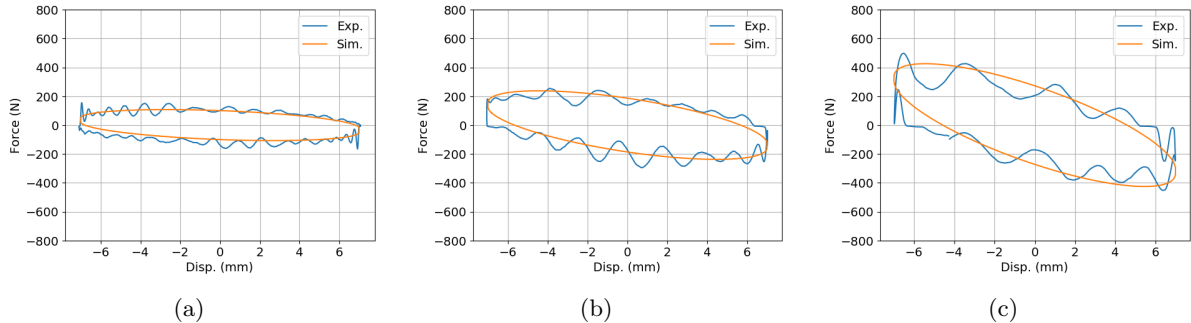


Figure 10: Force-displacement loops under harmonic vibration inputs of  $A=7\text{mm}$  for (a)  $\omega=1\text{Hz}$  (b)  $\omega=2\text{Hz}$  (c)  $\omega=3\text{Hz}$  with external electrical load  $R_e=10\Omega$  and the flywheel 2.

### 3.3 Energy Harvesting and Efficiency

The area of the force to displacement loop is the mechanical work done by the energy harvester on the input displacement of the testing machine. Therefore, the mechanical energy input by the testing machine can be written as

$$P_{input} = \frac{\omega}{2\pi} \cdot \Delta W \quad (16)$$

The energy collected by the harvester in one cycle can be calculated from the instantaneous harvesting power  $P_{captured} = V^2/R_e$ , period  $2\pi/\omega$  and the number of external resistors. The output power can be written as

$$P_{output} = 3 \times \frac{\int_0^{2\pi/\omega} P_{captured} dt}{2\pi/\omega} \quad (17)$$

With Equation 16 and 17, the total efficiency of this harvester  $\eta_{EH}$  can be calculated by

$$\eta_{EH} = \frac{P_{input}}{P_{output}} \quad (18)$$

The efficiency of converting mechanical energy into electrical energy  $P_e$  is its mechanical efficiency  $\eta_{Mech}$ , which can be expressed by

$$\eta_{Mech} = \frac{P_e}{P_{input}} \quad (19)$$

The electrical energy converted from mechanical energy can be split into two parts, that is, the collected power that can be collected in the external resistor and the power consumed in the internal resistance of the motor. It can be written as  $P_e = P_{captured} + P_{lost}$  where  $P_{captured} = R_e (i_1^2 + i_2^2 + i_3^2)$  and  $P_{lost} = R_i (i_1^2 + i_2^2 + i_3^2)$ . And the efficiency of converting electric energy to collecting power is electrical efficiency  $\eta_{Elec}$ . It can be expressed as

$$\eta_{Elec} = \frac{P_{captured}}{P_{captured} + P_{lost}} = \frac{R_e}{R_e + R_i} \quad (20)$$

Therefore, the total efficiency of the harvester can also be expressed by mechanical and electrical efficiencies. It can be written as

$$\eta_{EH} = \eta_{Mech} \eta_{Elec} \quad (21)$$

It can be known from Equation 18 and 20 that the total efficiency of the harvester can be calculated from the experimental results, and the electrical efficiency can be calculated from the ratio of the external resistor to the internal and external resistors.

If an experiment with three  $6.8\Omega$  resistors and an input sinusoidal displacement of 3Hz and an amplitude of 10mm is used as an example, the input power  $P_{input}=34.08W$  can be calculated by the loop of the result of the experiment in Figure 11(a). From Figure 11(b), the harvesting power  $P_{output}=13.24W$  is obtained and its instantaneous harvesting power is up to 19.11W.

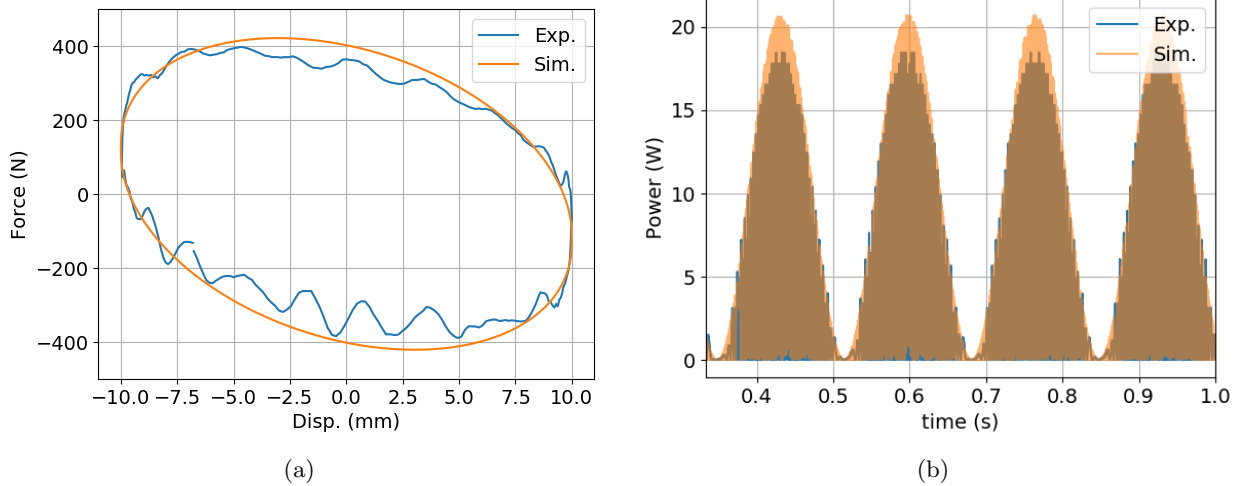


Figure 11: (a) Force-displacement loops (b) Phase power under harmonic vibration inputs of  $A=10\text{mm}$ ,  $\omega=3\text{Hz}$  with external electrical load  $R_e=6.8\Omega$

Since the internal resistance of the motor  $R_i=2.7\Omega$ , the total efficiency of the energy harvester is  $\eta_{EH}=0.388$ , and the electrical efficiency  $\eta_{Elec}=0.716$ , and then enter Equation 21 to calculate its mechanical efficiency  $\eta_{Mech}=0.542$ . The calculation of these efficiencies is mainly based on the experimental results of the harvester without the flywheel. It can be seen from Figure 12(a) that the higher the external resistance, the lower the mechanical efficiency, but Equation 20 shows that the electrical efficiency will be opposite. The external resistance of this paper is  $6.8\text{-}30\Omega$ , and the electrical efficiency is 71.6%-91.7%. Under the same input frequency of 3Hz and amplitude 10mm sinusoidal displacement, the mechanical efficiency is 54.3%-24.0%. In Figure 12(a), it can be found that the larger amplitude has higher mechanical efficiencies at the same frequency displacement, but as shown in Figure 12(b), the frequency is changed between 1-3Hz and the mechanical efficiency at the same amplitude. The impact is not great.

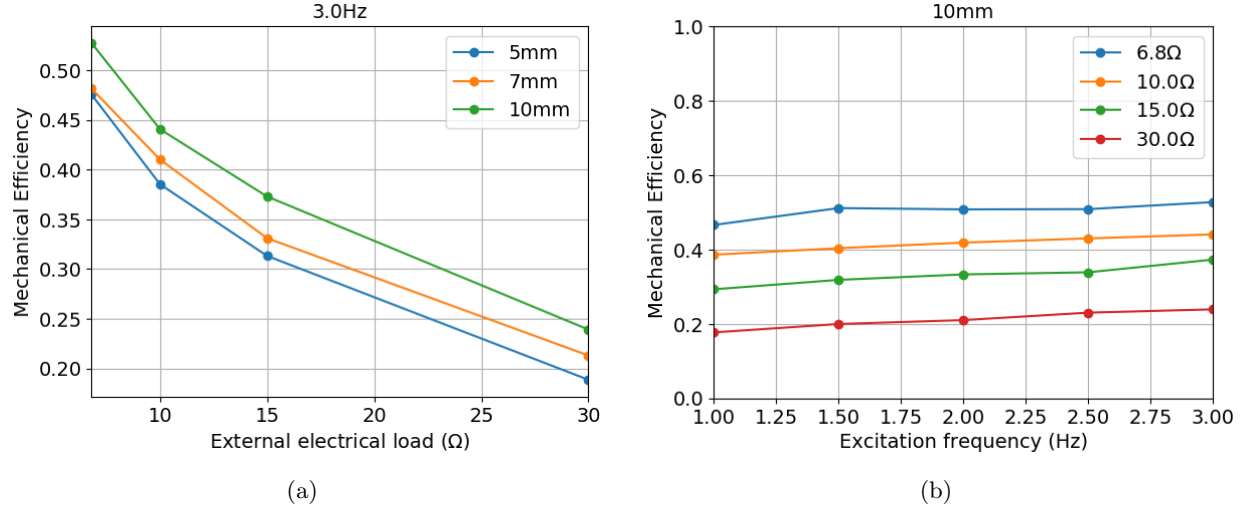


Figure 12: Mechanical efficiency (a) for different electrical loads and different amplitudes under vibration inputs of  $\omega=3\text{Hz}$ , (b) for different excitation frequencies and different electrical loads under vibration inputs of  $A=10\text{mm}$ .

Finally, the harvesting power and mechanical efficiency of different inertance are compared, and changing the inertance does not affect the harvesting power. In the case of the same input displacement as described above, three  $10\Omega$  resistors are connected, and the results are shown in Table 4. The output power of the one without flywheel and the two sets of equipped flywheels are  $11.03\text{W}$ ,  $11.06\text{W}$  and  $11.28\text{W}$ , respectively. The difference between the three is not significant, while the mechanical efficiency are  $47.54\%$ ,  $46.73\%$  and  $45.76\%$ , respectively. But the mechanical efficiency of the harvester with larger inertance is lower than the harvester with lower inertance. The main reason is that the input power is small without the addition of the flywheel. The three are  $29.46\text{W}$ ,  $30.07\text{W}$  and  $31.32\text{W}$ , respectively. But in terms of the increased inertance, the input power difference between the three is actually very small, so the results show that changing the inertance has little effect on the mechanical efficiency and the harvesting power.

Table 4: The efficiency of the energy harvesters

Parameters	Without Flywheel	Flywheel 1	Flywheel 2
$P_{input}$	$29.46 \text{ [W]}$	$30.07 \text{ [W]}$	$31.32 \text{ [W]}$
$P_{output}$	$11.03 \text{ [W]}$	$11.06 \text{ [W]}$	$11.28 \text{ [W]}$
$\eta_{Elec}$	0.79	0.79	0.79
$\eta_{Mech}$	0.48	0.47	0.46
$\eta_{EH}$	0.37	0.37	0.36

## 4 Case Study

This section will discuss the EH-TMDI model of a single-degree-of-freedom (SDOF) building system with the proposed electromagnetic energy harvester. The configuration is shown in Figure 13.

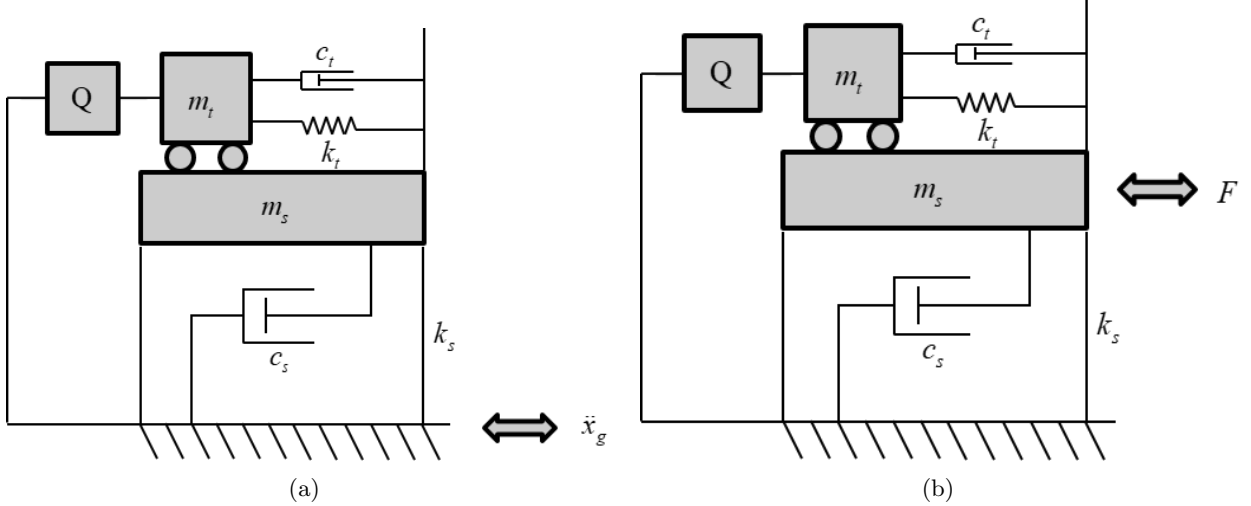


Figure 13: EH-TMDI is added to the SDOF system under (a) base (b) force excitation.

$Q$  represents the simplified ideal model of the proposed electromagnetic energy harvester. It can be regarded as the inertance  $b$  and the electromagnetic damping  $c_e$  of the harvester in parallel. The dynamic system can be expressed as

$$\begin{bmatrix} m_s & 0 \\ 0 & m_t + b \end{bmatrix} \begin{bmatrix} \ddot{x}_s \\ \ddot{x}_t \end{bmatrix} + \begin{bmatrix} c_s + c_t & -c_t \\ -c_t & c_t + c_e \end{bmatrix} \begin{bmatrix} \dot{x}_s \\ \dot{x}_t \end{bmatrix} + \begin{bmatrix} k_s & -k_t \\ -k_t & k_t \end{bmatrix} \begin{bmatrix} x_s \\ x_t \end{bmatrix} = F \quad (22)$$

where  $m_s$  and  $m_t$  are the primary structure mass and TMDI mass respectively,  $c_s$  and  $c_t$  are the primary structure damping coefficient and TMDI damping coefficient respectively,  $k_s$  and  $k_t$  are the primary structure stiffness and TMDI spring stiffness respectively,  $x_s$  and  $x_t$  are the displacement of the primary structure and the TMDI mass to the ground respectively, and  $F$  is the external force vector. If the earthquake causes the primary structure to vibrate, as shown in Figure 13(a), the external force vector can be expressed as

$$F = \begin{bmatrix} F_s \\ F_t \end{bmatrix} = - \begin{bmatrix} m_s \\ m_t \end{bmatrix} \ddot{x}_g \quad (23)$$

where  $F_s$  and  $F_t$  are the external forces to the primary structure and the external force to the TMDI mass, and  $\ddot{x}_g$  is the ground acceleration. If the primary structure is excited by the wind, that is, the external force acts only on the primary structure, as shown in Figure 13(b), the external force vector can be expressed as

$$F = \begin{bmatrix} F_s \\ 0 \end{bmatrix} \quad (24)$$

For the convenience of representation, the design variables commonly used in TMDI optimization are the primary structure damping ratio  $\zeta_s$ , the TMDI damping ratio  $\zeta_{tmdi}$ , the mass ratio  $\mu$ , the inertance ratio  $\beta$ , and the frequency ratio  $f_{tmdi}$ . The design variables described above will be described in detail below. The primary structure damping ratio is defined as  $\zeta_s = c_s/(2m_s\omega_s)$  where  $\omega_s$  is the natural frequency of the primary structure. The TMDI damping ratio is defined as  $\zeta_{tmdi} = c_t/(2m_t\omega_{tmdi})$  where  $\omega_{tmdi}$  is the natural frequency of the TMDI, and it can be written as  $\omega_{tmdi} = \sqrt{k_t/(m_t + b)}$ . When the TMDI damping ratio is too large, the connection between the TMDI and the primary structure is too strong, and the TMDI is almost integrated with the primary structure, thereby causing the reaction to be amplified. When the TMDI damping ratio is too small, the damping effect is not good. And the reaction of TMD itself will be too large. The mass ratio can be expressed as  $\mu = m_t/m_s$ . The inertance ratio is  $\beta = b/m_s$ . And the frequency ratio is defined as the ratio of the natural frequency of the TMDI to the natural frequency of the primary structure, expressed

as  $f_{tmdi} = \omega_{tmdi}/\omega_s$ . This paper uses the built-in Simscape in MATLAB/SIMULINK to build a single-storey building model. The parameters are shown in Table 5 and 6. Next, the real seismic signal will be used as the ground acceleration input and the simulated fluctuating wind speed as the wind force input to analyze the vibration reduction performance and energy harvesting of EH-TMDI.

Table 5: The parameters of the SDOF building system with EH-TMDI

Parameters	Values	Description
$m_s$	50000 [kg]	Mass of the primary structure
$\omega_s$	1 [Hz]	Natural frequency of the primary structure
$\zeta_s$	0.02	Damping ratio of the primary structure
$\mu$	0.01	Mass ratio
$\beta$	0.1 & 0.3	Inertance ratio

Table 6: The optimal design variables of TMDI under simple harmonic vibration [39]

Parameters	Base-excited	Force-excited
$f_{tmdi}$	$\frac{1}{1+\mu+\beta} \sqrt{\frac{(1+\mu)(2-\mu)-\mu\beta}{2(1+\mu)}}$	$\frac{1}{1+\mu+\beta}$
$\zeta_{tmdi}$	$\sqrt{\frac{\beta^2\mu+6\mu(1+\mu)^2+\beta(1+\mu)(6+7\mu)}{8(1+\mu)(1+\mu+\beta)[2+\mu(1-\mu-\beta)]}}$	$\sqrt{\frac{3(\mu+\beta)}{8(1+\mu+\beta)}}$

#### 4.1 Energy Harvesting in Base-Excited TMDI Equipped Structures

This paper selects the horizontal direction vibration signal of each earthquake to carry out the case analysis of the vibration reduction and energy harvesting, and selects four seismic records in the PEER Ground Motion Database for earthquake analysis, namely Kobe Japan KAK000, Chi-Chi Taiwan CHY008-N, Duzce Turkey BOL090 and San Fernando California PUL164, as shown in Figure 14. This case study connects three  $3.3\Omega$  external resistors  $R_e$  with a Y-connection, so its  $c_e$  can be calculated by

$$c_e = \left( \frac{2\pi}{p} \right)^2 \frac{3k_e k_t}{2R} r_g \quad (25)$$

Since the main structure is forced to dissipate energy by the mass vibration of EH-TMDI, the vibration energy generated by the mass for energy dissipation is converted into electric energy by the energy harvester, which is calculated by the velocity of the TMDI mass. The  $\dot{x}_t$  is substituted into  $\omega = (2\pi/p)v$  to obtain the angular velocity of the gearbox rotor and then substitutes  $\omega_g$  in Equations 5 and 6 to obtain the three-phase current of the motor. Finally, one of the phase currents is substituted into  $P_{captured} = i^2 R_e$  to obtain the single-phase harvesting power. The simulation results of the four seismic records can be seen in Figure 15 and 16. From the results, it can be seen that the addition of EH-TMDI can effectively reduce the vibration. If we compare the two inertance ratio  $\beta$ , it can be found that the  $\beta$  boost can make the damping effect better, but because of the velocity of the TMDI mass reduced, so the harvesting power will also drop.

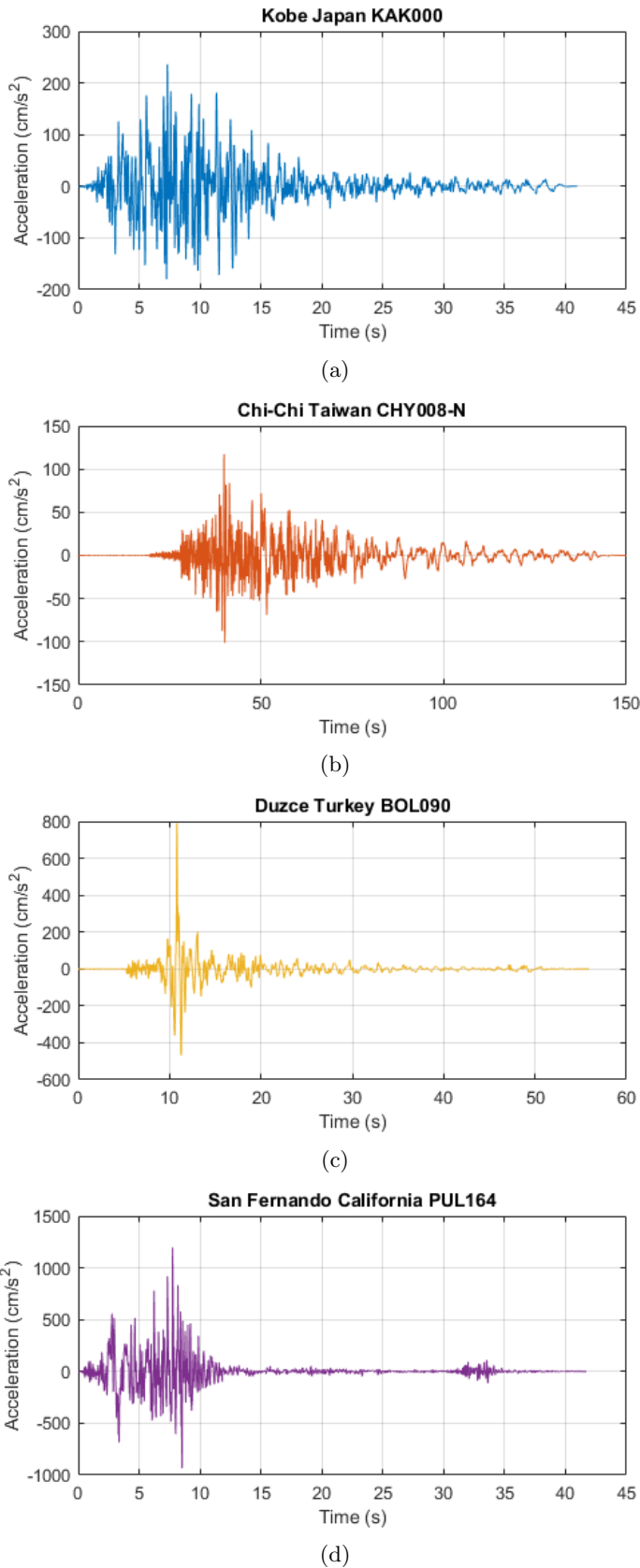
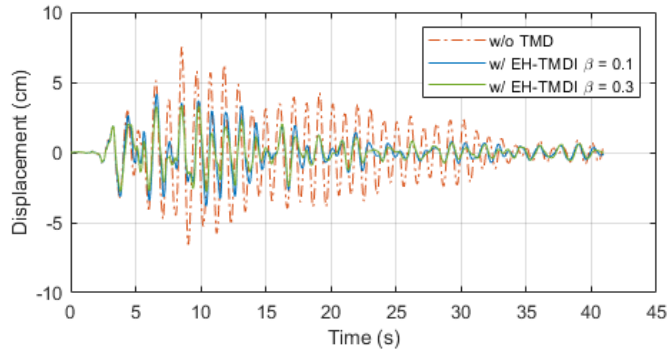
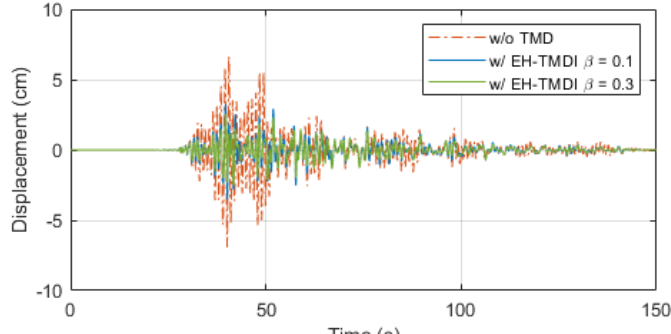


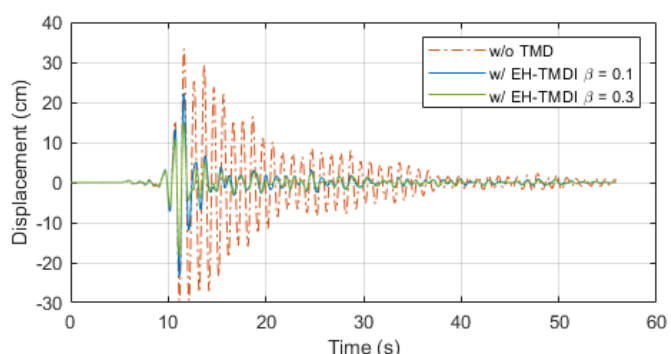
Figure 14: The ground acceleration of seismic records of (a) Kobe Japan KAK000 (b) Chi-Chi Taiwan CHY008-N (c) Duzce Turkey BOL090 (d) San Fernando California PUL164



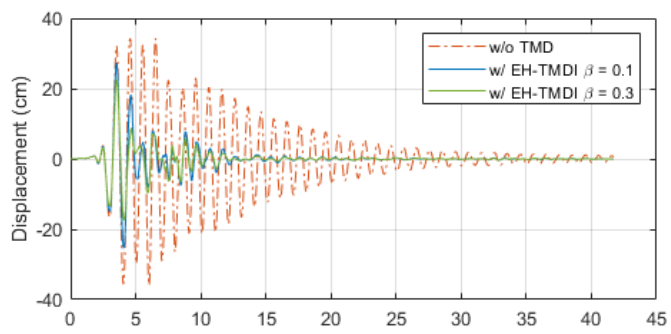
(a)



(b)

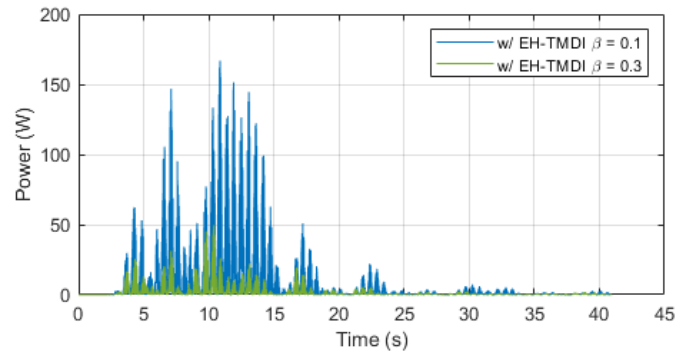


(c)

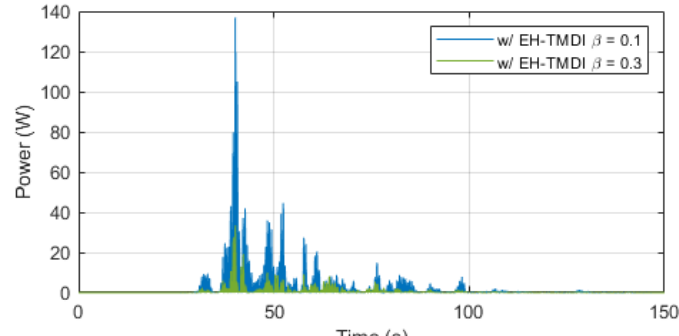


(d)

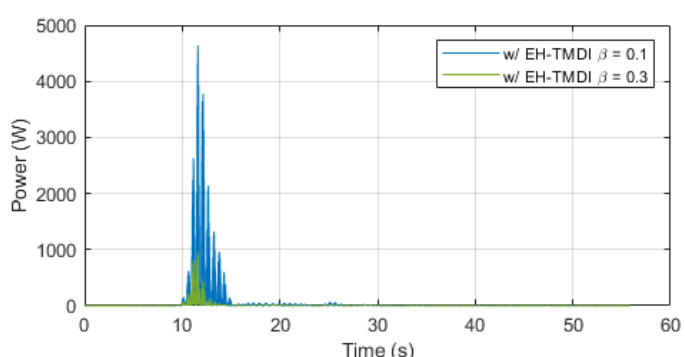
Figure 15: The displacement of the main structure under seismic records of (a) Kobe Japan KAK000 (b) Chi-Chi Taiwan CHY008-N (c) Duzce Turkey BOL090 (d) San Fernando California PUL164



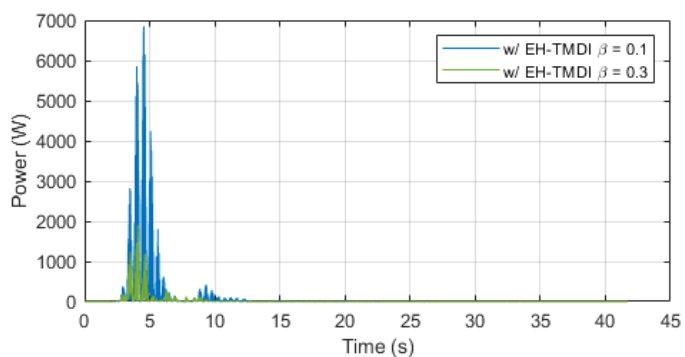
(a)



(b)



(c)



(d)

Figure 16: The harvesting power under seismic records of (a) Kobe Japan KAK000 (b) Chi-Chi Taiwan CHY008-N (c) Duzce Turkey BOL090 (d) San Fernando California PUL164

## 4.2 Energy Harvesting in Force-Excited TMDI Equipped Structures

In addition to being effective in damping earthquakes, EH-TMDI can also be used to resist wind. The external force vector is shown in Equation 24 where  $F_s$  is the wind input acting on the main structure. Since the wind action is a long-term external force, such as expressing the wind force as the average wind force plus the fluctuating wind force, the simulation process represents the direct application of wind force on the static building, and the result is a transient solution. That is, the building will only have a large vibration displacement at the beginning, but it will gradually become flatter. This result will not be consistent with the actual situation, because the average wind force will cause a offset of the main structure of the building. Therefore, the reference [41] in this paper uses fluctuating wind force as the wind force input, and its equation can be expressed as

$$F_s = \rho \cdot C_D \cdot A \cdot V_{10} \cdot u \quad (26)$$

where the air density is  $\rho=1.28\text{kg/m}^3$  and the drag coefficient is  $C_D=1.2$ . It is assumed that the wind is at a height of 10m from the ground, and its wind receiving area is  $A=100\text{m}^2$ , and  $V_{10}$  is the average wind speed at 10m high. It is taken as 42.5m/s and 19.55m/s, which means that 50-year and 1-year return period brings averaged over 10 minutes at a height of 10m. And  $u$  is the fluctuating wind speed. Figure 17(a) is the fluctuating wind time history generated, whose duration is 600s and the time interval is 0.1s. As shown in Figure 17(b), the generated wind time history is converted to power spectral density by FFT, which is compared with the target Kaimal spectrum. It is shown that the peak value is not at 1Hz. Therefore, the resonance reaction can be ignored.

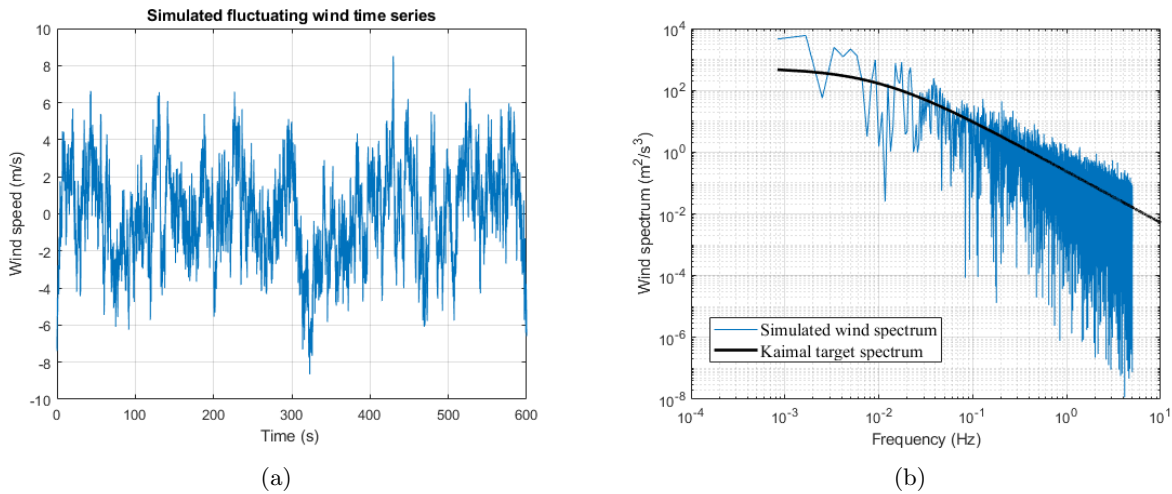


Figure 17: Simulated fluctuating wind time history: (a) wind speed and (b) power spectrum.

Finally, Figure 18 shows the damping effect of EH-TMDI. Figure 19 shows the harvesting power of EH-TMDI, but the 50-year return period winds are less frequent. Therefore, the analysis result of wind in one year's return period will be more objective. Combining the results of the two, it can be seen that EH-TMDI is also suitable for energy harvesting when resisting wind, and its relationship with the inertance is also the same as that in the seismic force time history response. Although the harvesting power is much smaller than the seismic force, the peak value of its single phase harvesting power is not more than 100W, but the wind is more often used on the primary structure of the building than the seismic force. In the future, the two conditions can be optimized separately to make it better for energy harvesting under certain conditions.

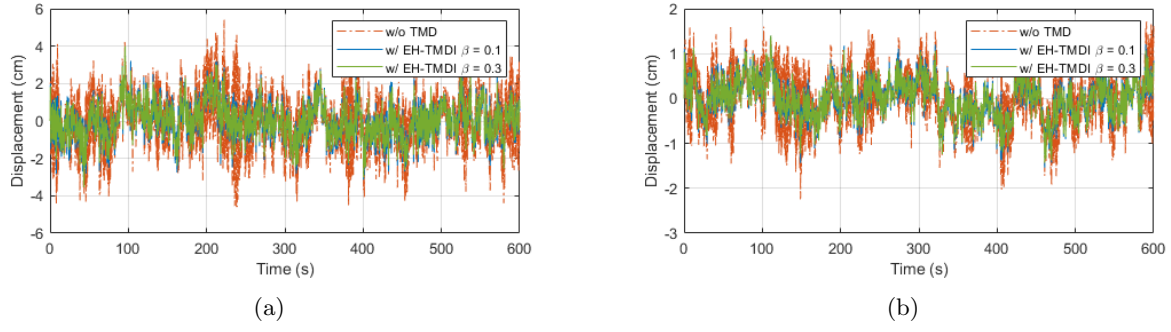


Figure 18: Time-history responses of displacements of the primary structure as (a) 50-year and (b) 1-year return period  $V_{10}$  input

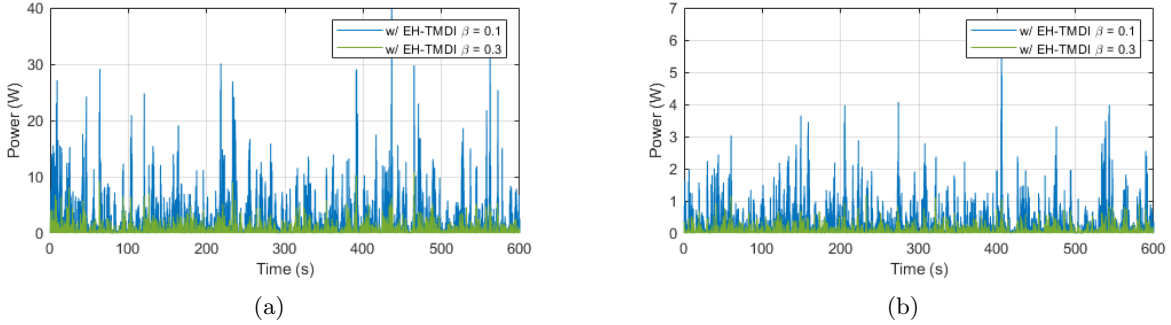


Figure 19: Harvesting power as (a) 50-year and (b) 1-year return period  $V_{10}$  input

## 5 Conclusion

In this article, the dynamic behavior of the proposed electromagnetic energy harvester is studied by inputting the sinusoidal displacement. The method of changing the external resistance and the inertance is used to adjust the equivalent damping and equivalent stiffness of the harvester to achieve that the vibration of the target system can be dissipated while storing energy. The main results of this research are as follows. First, a parametric electromagnetic energy harvester is established. The mathematical model is verified by the dynamic testing machine, which is convenient for future researchers to study. Secondly, the proposed electromagnetic energy harvester is simulated in TMDI by numerical simulation, and its reduction effect and energy harvesting power under vibration duration response is analyzed. In order to facilitate the analysis, this paper divided the experimental verification into four parts, first verifying the friction of the ball screw, and then verifying the motor damping coefficient after connecting the ball screw to the three-phase brushless motor, followed by adjusting the external resistors and analyzing the equivalent damping of the harvester, and finally change the inertance and analyze its effect.

## References

- [1] Z. Jin-qiu, P. Zhi-zhao, Z. Lei, and Z. Yu, “A review on energy-regenerative suspension systems for vehicles,” in *Proceedings of the World Congress on Engineering*, vol. 3, pp. 3–5.
- [2] L. H. Fang, S. I. S. Hassan, R. B. A. Rahim, and M. F. A. Malek, “A study of vibration energy harvester,” *ARPJ Journal of Engineering and Applied Sciences*, vol. 11, no. 8, pp. 5028–5041, 2016.
- [3] D. Karnopp, “Permanent magnet linear motors used as variable mechanical dampers for vehicle suspensions,” *Vehicle System Dynamics*, vol. 18, no. 4, pp. 187–200, 1989.

- [4] I. Martins, J. Esteves, G. D. Marques, and F. P. Da Silva, “Permanent-magnets linear actuators applicability in automobile active suspensions,” *IEEE Transactions on vehicular technology*, vol. 55, no. 1, pp. 86–94, 2006.
- [5] Y. Suda and T. Shiiba, “A new hybrid suspension system with active control and energy regeneration,” *Vehicle System Dynamics*, vol. 25, no. S1, pp. 641–654, 1996.
- [6] K. Nakano and Y. Suda, “Combined type self-powered active vibration control of truck cabins,” *Vehicle System Dynamics*, vol. 41, no. 6, pp. 449–473, 2004.
- [7] K. Nakano, Y. Suda, and S. Nakadai, “Self-powered active vibration control using a single electric actuator,” *Journal of Sound and Vibration*, vol. 260, no. 2, pp. 213–235, 2003.
- [8] A. Gupta, J. A. Jendrzejczyk, T. M. Mulcahy, and J. R. Hull, “Design of electromagnetic shock absorbers,” *International Journal of Mechanics and Materials in Design*, vol. 3, no. 3, pp. 285–291, 2006.
- [9] B. L. Gysen, T. P. van der Sande, J. J. Paulides, and E. A. Lomonova, “Efficiency of a regenerative direct-drive electromagnetic active suspension,” *IEEE transactions on vehicular technology*, vol. 60, no. 4, pp. 1384–1393, 2011.
- [10] C. Chao and L. Wei-Hsin, “A self-sensing magnetorheological damper with power generation,” *Smart Materials and Structures*, vol. 21, no. 2, p. 025014, 2012.
- [11] Z. Lei, S. Brian, S. Jurgen, and Z. Yu, “Design and characterization of an electromagnetic energy harvester for vehicle suspensions,” *Smart Materials and Structures*, vol. 19, no. 4, p. 045003, 2010.
- [12] X. Tang, T. Lin, and L. Zuo, “Design and optimization of a tubular linear electromagnetic vibration energy harvester,” *IEEE/ASME Transactions on Mechatronics*, vol. 19, no. 2, pp. 615–622, 2014.
- [13] M. Yuan, K. Liu, and A. Sadhu, “Simultaneous vibration suppression and energy harvesting with a non-traditional vibration absorber,” *Journal of Intelligent Material Systems and Structures*, p. 1045389X17754263, 2018.
- [14] Z. Li, L. Zuo, G. Luhrs, L. Lin, and Y.-x. Qin, “Electromagnetic energy-harvesting shock absorbers: Design, modeling, and road tests,” *IEEE Transactions on Vehicular Technology*, vol. 62, no. 3, pp. 1065–1074, 2013.
- [15] Z. Li, L. Zuo, J. Kuang, and G. Luhrs, “Energy-harvesting shock absorber with a mechanical motion rectifier,” *Smart Materials and Structures*, vol. 22, no. 2, p. 025008, 2012.
- [16] X. Tang and L. Zuo, “Simultaneous energy harvesting and vibration control of structures with tuned mass dampers,” *Journal of Intelligent Material Systems and Structures*, vol. 23, no. 18, pp. 2117–2127, 2012.
- [17] Y. Pan, F. Liu, R. Jiang, Z. Tu, and L. Zuo, “Design, modeling and lab test of electromagnetic energy harvester for railway vehicle suspensions,” in *ASME 2017 International Design Engineering Technical Conferences and Computers and Information in Engineering Conference*, pp. V003T01A018–V003T01A018, American Society of Mechanical Engineers.
- [18] J. Wang, T. Lin, and L. Zuo, “High efficiency electromagnetic energy harvester for railroad application,” in *ASME 2013 International Design Engineering Technical Conferences and Computers and Information in Engineering Conference*, pp. V004T08A037–V004T08A037, American Society of Mechanical Engineers.
- [19] T. Lin, Y. Pan, S. Chen, and L. Zuo, “Modeling and field testing of an electromagnetic energy harvester for rail tracks with anchorless mounting,” *Applied Energy*, vol. 213, pp. 219–226, 2018.
- [20] M. Liu, R. Lin, S. Zhou, Y. Yu, A. Ishida, M. McGrath, B. Kennedy, M. Hajj, and L. Zuo, “Design, simulation and experiment of a novel high efficiency energy harvesting paver,” *Applied Energy*, vol. 212, pp. 966–975, 2018.

- [21] Y. Kawamoto, Y. Suda, H. Inoue, and T. Kondo, “Modeling of electromagnetic damper for automobile suspension,” *Journal of System Design and Dynamics*, vol. 1, no. 3, pp. 524–535, 2007.
- [22] Y. Kawamoto, Y. Suda, H. Inoue, and T. Kondo, “Electro-mechanical suspension system considering energy consumption and vehicle manoeuvre,” *Vehicle System Dynamics*, vol. 46, no. S1, pp. 1053–1063, 2008.
- [23] Y. Zhang, K. Huang, F. Yu, Y. Gu, and D. Li, “Experimental verification of energy-regenerative feasibility for an automotive electrical suspension system,” in *Vehicular Electronics and Safety, 2007. ICVES. IEEE International Conference on*, pp. 1–5, IEEE.
- [24] I. L. Cassidy, J. T. Scruggs, S. Behrens, and H. P. Gavin, “Design and experimental characterization of an electromagnetic transducer for large-scale vibratory energy harvesting applications,” *Journal of Intelligent Material Systems and Structures*, vol. 22, no. 17, pp. 2009–2024, 2011.
- [25] I. L. Cassidy and J. T. Scruggs, “A statistical linearization approach to optimal nonlinear energy harvesting,” in *Proc. of SPIE*, vol. 8341, pp. 834105–1 – 834105–12.
- [26] C. K. Wai and Y. Y. Rong, “Electric vehicle energy harvesting system regenerative shock absorber for electric vehicle,” in *Sustainable Utilization and Development in Engineering and Technology (CSUDET), 2013 IEEE Conference on*, pp. 7–10, IEEE.
- [27] Y. Liu, L. Xu, and L. Zuo, “Design, modeling, lab and field tests of a mechanical-motion-rectifier-based energy harvester using a ball-screw mechanism,” *IEEE/ASME Transactions on Mechatronics*, vol. 22, no. 5, pp. 1933–1943, 2017.
- [28] A. Maravandi and M. Moallem, “Regenerative shock absorber using a two-leg motion conversion mechanism,” *IEEE/ASME Transactions on Mechatronics*, vol. 20, no. 6, pp. 2853–2861, 2015.
- [29] M. C. Smith and F.-C. Wang, “Performance benefits in passive vehicle suspensions employing inerters,” *Vehicle System Dynamics*, vol. 42, no. 4, pp. 235–257, 2004.
- [30] F.-C. Wang, C.-H. Yu, M.-L. Chang, and M. Hsu, “The performance improvements of train suspension systems with inerters,” in *Proceedings of the IEEE Conference on Decision and Control*, pp. 1472–1477.
- [31] M. Hsu, *The realisations of Inerter concept and the application to building suspension*. M.s. thesis, 2005.
- [32] C.-H. Lee, *Applications of Inerter Networks for Vibration Suppression of Milling Machine Tools*. M.s. thesis, 2017.
- [33] F.-C. Wang and W.-J. Su, “Impact of inerter nonlinearities on vehicle suspension control,” *Vehicle system dynamics*, vol. 46, no. 7, pp. 575–595, 2008.
- [34] F. C. Wang, M. F. Hong, and T. C. Lin, “Designing and testing a hydraulic inerter,” *Proceedings of the Institution of Mechanical Engineers, Part C: Journal of Mechanical Engineering Science*, vol. 225, no. 1, pp. 66–72, 2010.
- [35] F.-C. Wang and H.-A. Chan, “Mechatronic suspension design and its applications to vehicle suspension control,” in *Proceedings of the IEEE Conference on Decision and Control*, pp. 3769–3774.
- [36] H.-J. Chen, W.-J. Su, and F.-C. Wang, “Modeling and analyses of a connected multi-car train system employing the inerter,” *Advances in Mechanical Engineering*, vol. 9, no. 8, p. 1687814017701703, 2017.
- [37] L. Marian and A. Giaralis, “Optimal design of a novel tuned mass-damper-inerter (tmdi) passive vibration control configuration for stochastically support-excited structural systems,” *Probabilistic Engineering Mechanics*, vol. 38, pp. 156–164, 2014.
- [38] J. Salvi and A. Giaralis, “Concept study of a novel energy harvesting-enabled tuned mass-damper-inerter (eh-tmdi) device for vibration control of harmonically-excited structures,” in *Journal of Physics: Conference Series*, vol. 744, p. 012082, IOP Publishing.

- [39] L. Marian and A. Giaralis, “The tuned mass-damper-inerter for harmonic vibrations suppression, attached mass reduction, and energy harvesting,” *Smart structures and systems*, vol. 19, no. 6, pp. 665–678, 2017.
- [40] T.-C. Hung, G.-L. Lin, C.-C. Lin, Y. Liu, and L. Zuo, “Vibration control of seismic structures using electromagnetic multiple tuned mass dampers with rotary transducers,” in *The 2017 World Congress on Advances in Structural Engineering and Mechanics (ASEM17)*.
- [41] Y. Luo, H. Sun, X. Wang, L. Zuo, and N. Chen, “Wind induced vibration control and energy harvesting of electromagnetic resonant shunt tuned mass-damper-inerter for building structures,” *Shock and Vibration*, vol. 2017, 2017.
- [42] J. E. Shigley, *Shigley's mechanical engineering design*. Tata McGraw-Hill Education, 2011.
- [43] H.-A. Chan, *The Design and Application of the Mechatronic Suspension Systems*. M.s. thesis, 2008.